Supplementary Material

Fused-ring Electron Acceptor Molecules with Narrow Bandgap for Near-infrared Broadband Ultrafast Laser Absorption

Jiabei Xu[1], Xingzhi Wu[2*], Wenfa Zhou[3], Tianwei Zhang[3], Junyi Yang[1], Li Jiang[4*], Yinglin Song[1,3*]

[1]School of Physical Science and Technology, Soochow University, Suzhou, 215006, China
[2]Jiangsu Key Laboratory of Micro and Nano Heat Fluid Flow Technology and Energy Application, School of Physical Science and Technology, Suzhou University of Science and Technology, Suzhou, 215009, China
[3]Department of Physics, Harbin Institute of Technology, Harbin, 150001, China
[4]Beijing National Laboratory for Molecular Science, Key Laboratory of Molecular Nanostructure and nanotechnology, Institute of Chemistry Chinese Academy of Sciences, Beijing, 100190, China

Contents

1. UV-Vis-NIR absorption and fluorescence spectra of ITIC-4F and IEICO-4F under different concentrations

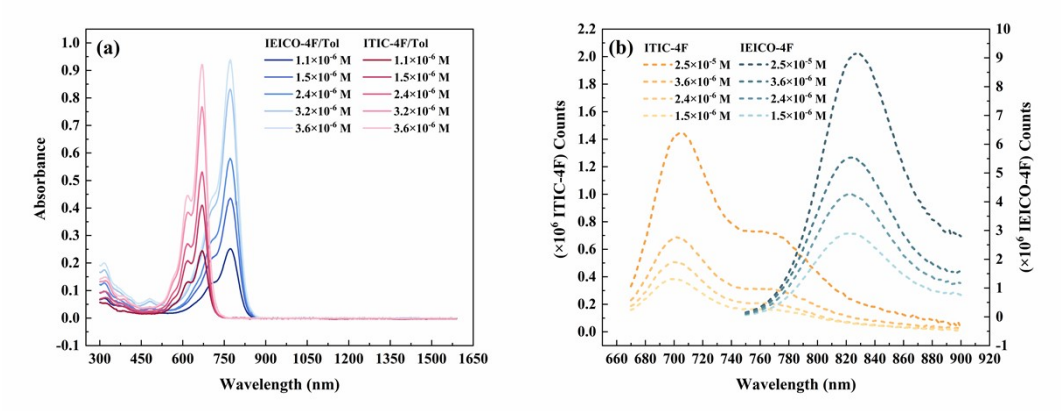

Figure S1 The UV-Vis-NIR absorption (a) and fluorescence spectra (b) of ITIC-4F and IEICO-4F under different concentrations.

2. Dynamic curves around 950 nm of IEICO-4F and 800 nm of ITIC-4F extracted from TAS.

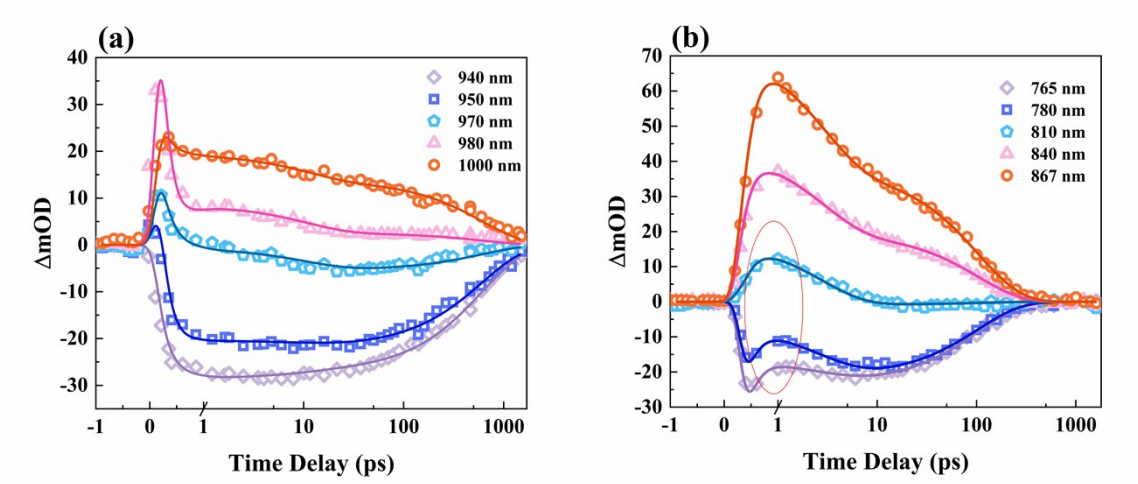

Figure S2 The transient absorption dynamic curves of IEICO-4F at 940 nm, 950 nm, 970 nm, 980 nm and 1000 nm (a) and the transient absorption dynamic curves of ITIC-4F at 765 nm, 780 nm, 810 nm, 840 nm and 867 nm.

To analyze the assignment of the signal around 950 nm in TAS, we extract the transient absorption dynamic curves at 940 nm, 950 nm, 970 nm, 980 nm and 1000 nm in Figure 3. The linear absorption of IEICO-4F can be ignored at 950 nm, and the saturable absorption signal can be attributed to the stimulated emission (SE) at 940 nm and 950 nm. After 960 nm, the dynamic curves exhibit the competition between excited-state absorption (ESA) and SE. With the decrease of the fluorescence, the ESA on the local excited state (LES) prevail the SE during the initial time. Then the accumulation of electrons on the fluorescence level makes the SE apparent. However, after the electrons rapidly transfer to the intramolecular charge transfer state (ICT) (after ~ 10 ps), the excited-state absorption on the ICT state gradually cancels out the negative signal generated by SE (970 nm, 980 nm). After

around 1000 nm, the dynamic curves change obviously, and the positive signal is entirely generated from excited state absorption.

The excited state dynamics of ITIC-4F are similar to IEICO-4F. However, the electrons on the excited states of ITIC-4F relax more rapidly than IEICO-4F, and the intensity of SE is smaller, which is consistent with the fluorescence spectra in Figure S1 (b). Therefore, the competition between ESA and SE is not as obvious as that in the IEICO-4F, but we can still observe the transient signal which represents the competition in Figure S2 (b) (marked by the red circle at 765 nm-810 nm). After 810 nm, The positive signal can be attributed to ESA.

3. Femtosecond open-aperture (OA) Z-Scan curves of IEICO-4F

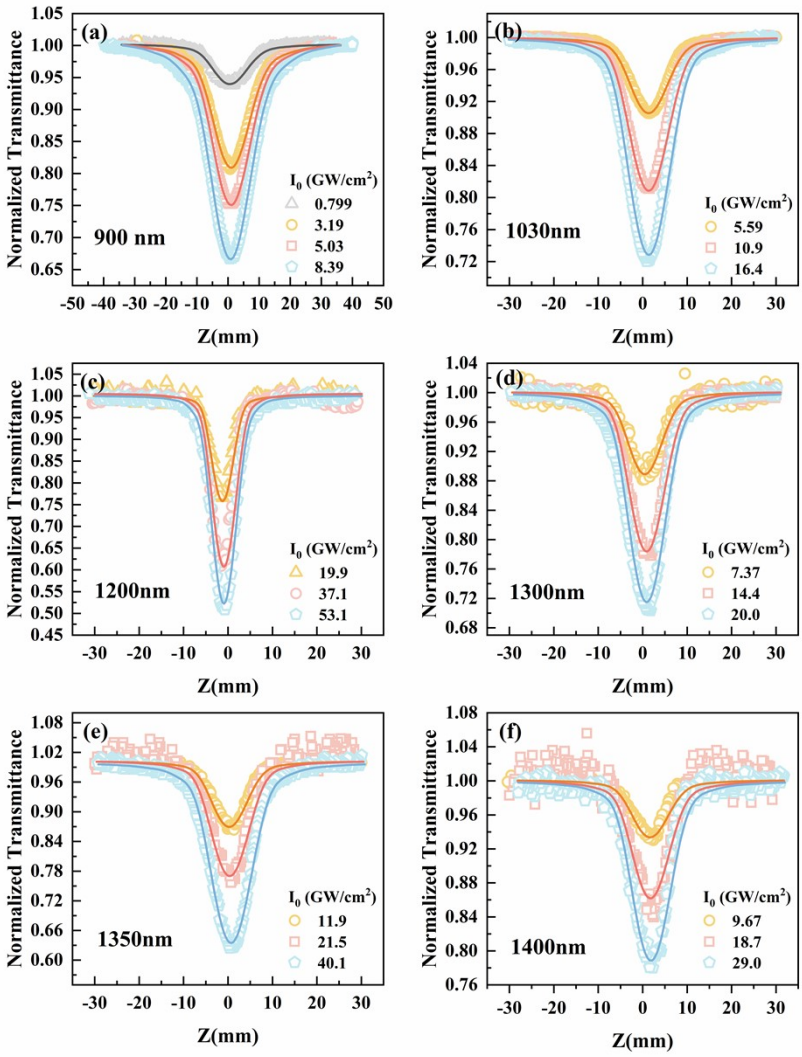

Figure S3 Femtosecond open-aperture Z-scan curves of IEICO-4F. The solid lines represent numerical fitting.

4. Femtosecond OA Z-Scan curves of ITIC-4F

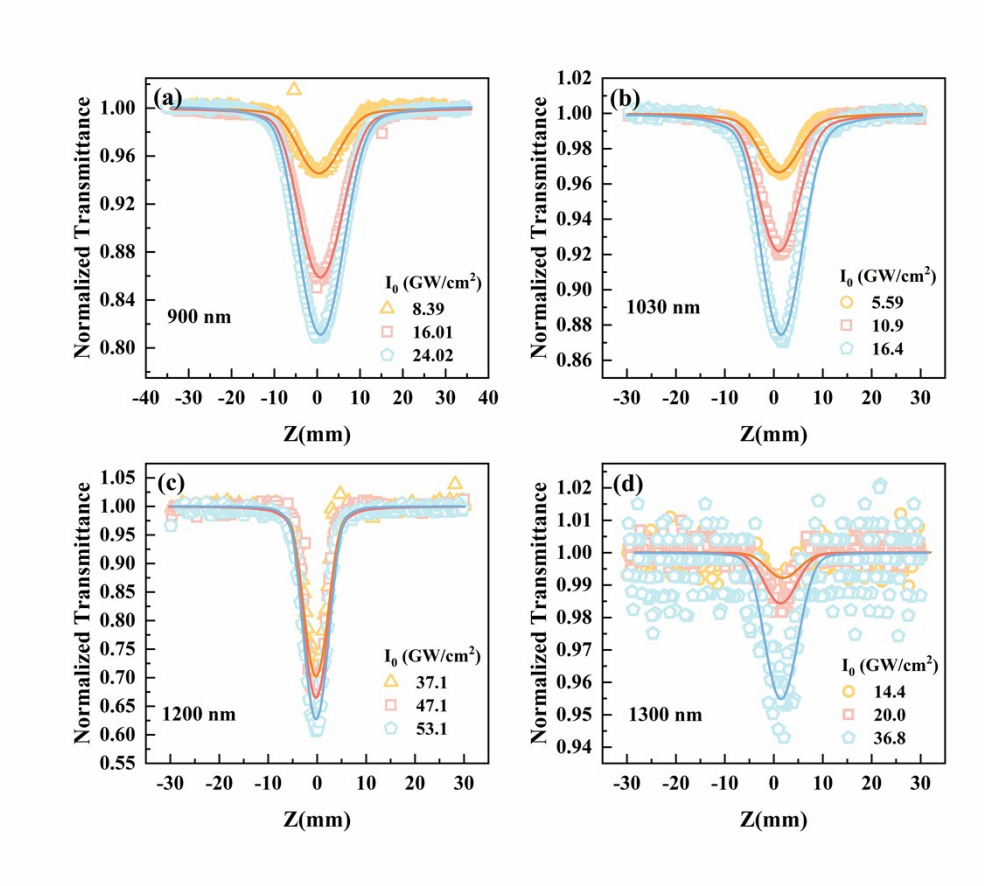

Figure S4 Femtosecond open aperture Z-scan curves of ITIC-4F. The solid lines represent numerical fitting.

5. Nonlinear absorption coefficients as a function of input laser intensity at measured wavelengths of both compounds

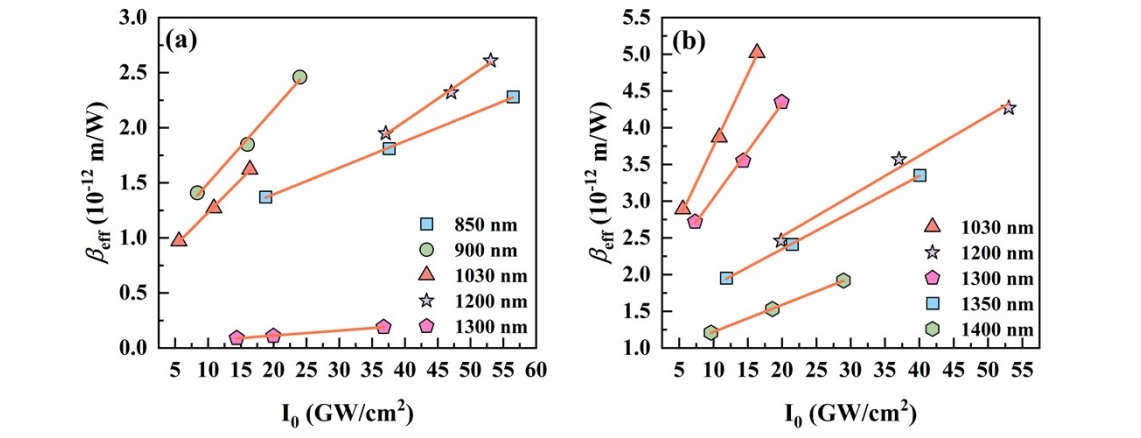

Figure S5 Nonlinear absorption coefficients as a function of input laser intensity at measured wavelengths for (a) ITIC-4F and (b) IEICO-4F.

6. Phase-Object pump probe

The time-resolved degenerate phase-object pump probe (POPP) technique is a combination of traditional pump-probe and 4f coherent imaging[1], which can measure the NLA and NLR simultaneously. A transparent dielectric plate with a transparent layer (phase-object PO) in its center is placed on the front focal surface of 4f system. The layer with a thickness of 1/4 of the measured wavelength is used to generate an additional phase of 0.5π. The probe laser beam modulated by the PO is focused through the sample and the nonlinear phase shift caused by laser pumping may produce the changes of the intensity in the radius of PO. The details of experimental setup can be found elsewhere[2]. In this investigation, POPP is used to vertify the nonlinear absorption and refraction mechanisms of both compounds in the near-resonance and two-photon absorption regions.

7. Transient absorption and refraction kinetics of IEICO-4F and ITIC-4F at 850 nm

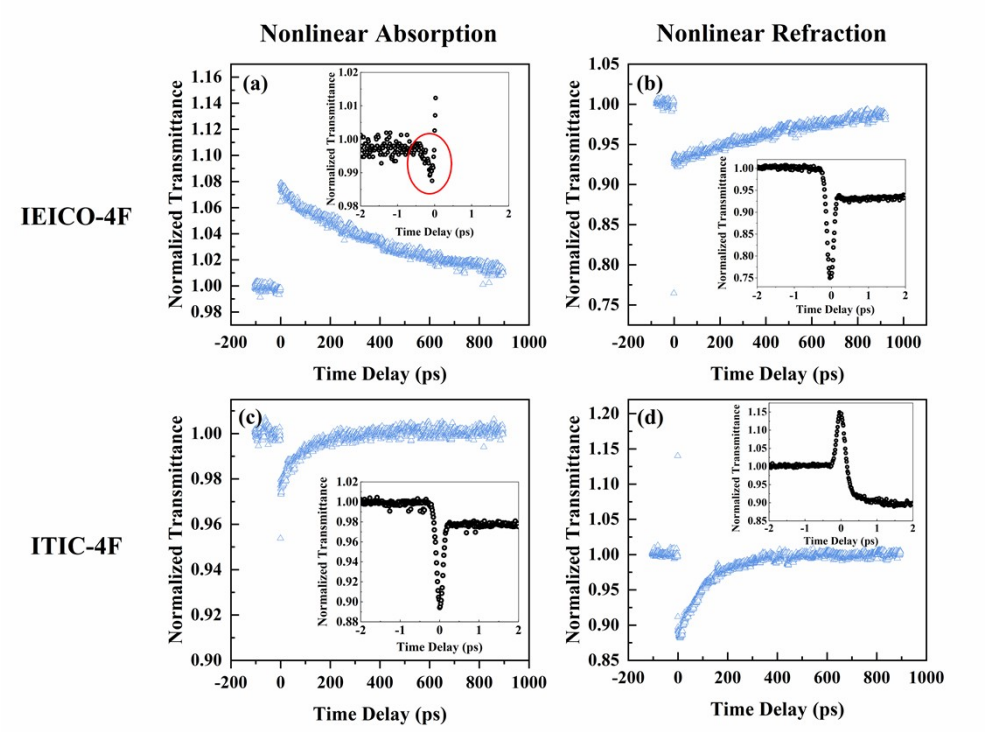

Figure S6 The transient nonlinear absorption and refraction dynamics of both compounds at 850 nm. (a) & (c) are transient nonlinear absorption dynamic trances of **IEICO-4F** and **ITIC-4F**, respectively. (b) & (d) are transient nonlinear refraction dynamic traces of **IEICO-4F** and **ITIC-4F**, respectively. The inset graphs are early kinetics of the short time delay within the first 2 ps.

8. Transient absorption and refraction kinetics of IEICO-4F and ITIC-4F at 1030 nm

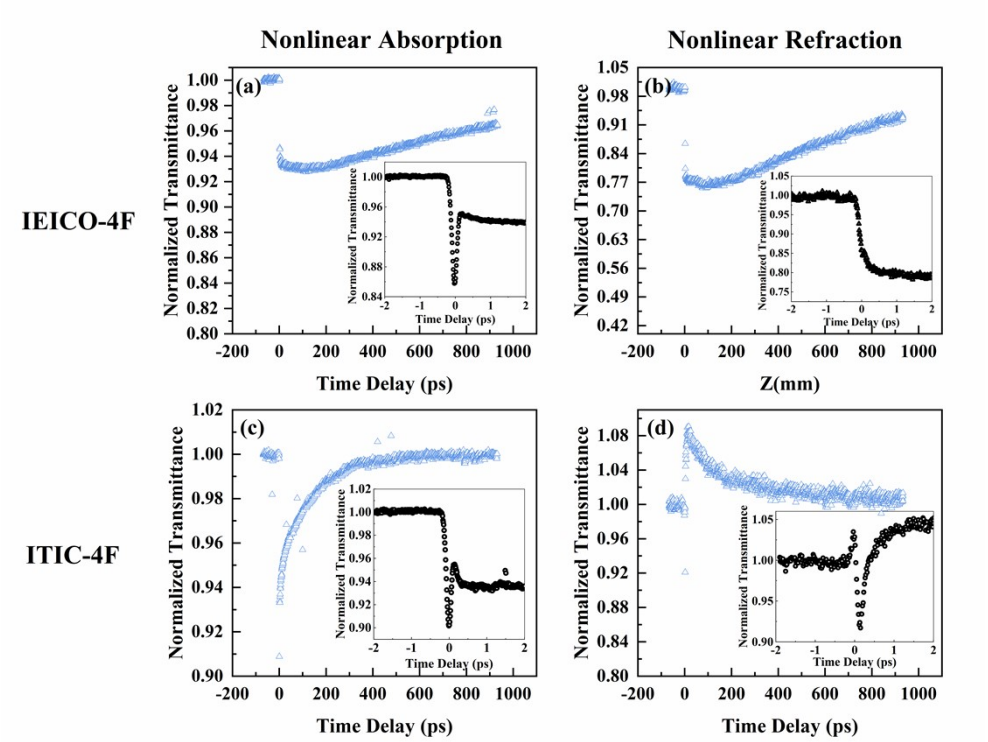

Figure S7 The transient nonlinear absorption and refraction dynamics of both compounds at 1030 nm. (a) & (c) are transient nonlinear absorption dynamic trances of **IEICO-4F** and **ITIC-4F**, respectively. (b) & (d) are transient nonlinear refraction dynamic traces of **IEICO-4F** and **ITIC-4F**, respectively. The inset graphs are early kinetics of the short time delay within the first 2 ps.

9. The NLO parameters of IEICO-4F at 850 nm and 900 nm for numerical fitting in Z-Scan

Table S1 The NLO parameters extracted from Z-scan at 850 nm and 900 nm of IEICO-4F. The third-order polarizability $\chi^{(3)}$ and second-order hyperpolarizability γ' are calculated.

Wavelength (nm)	I_0 (GW/cm^2)	I_s (GW/cm^2)	α_2 (10^{-12} m/W)	Im{$\chi^{(3)}$} (10^{-13} esu)	*n* eff 2 (10^{-6} cm^2/GW)	Re{$\chi^{(3)}$} (10^{-13} esu)	γ' (10^{-30} esu)
850	0.941	1.21	3.85	1.41	-15.1	-8.19	1.72
	1.88	1.21	3.85	1.41	-15.5	-8.40	1.77
900	3.19	-	13.1	5.09	-13.7	-7.43	0.37
	5.03	-	13.1	5.09	-14.7	-7.97	0.39
	8.39	-	13.2	5.13	-16.9	-9.16	0.43

The third-order polarizability $\chi^{(3)}$ and second-order hyperpolarizability γ' can be calculated by the following Equation 1-4:

$$\mathrm{Re}\{\chi^{(3)}\} = \frac{{n_0}^2 c}{120\pi^2} n_2^{eff} \quad (1)$$

$$\mathrm{Im}\{\chi^{(3)}\} = \frac{{n_0}^2 c^2}{240\pi^2 \omega} \beta_{eff} \quad (2)$$

$$\left|\chi^{(3)}\right| = \left|\mathrm{Re}\{\chi^{(3)}\} + \mathrm{Im}\{\chi^{(3)}\}\right| \quad (3)$$

$$\left|\gamma^{'}\right| = \frac{\left|\chi^{(3)}\right|}{Nf^4} \quad (4)$$

In these equations, $f = (n_0^2 + 2)/3$ refers to the local field factor, N represents population density per cubic centimeter, and ω is angular frequency.

10. Effective nonlinear absorption coefficients extracted from Z-Scan measurements

Table S2 Effective nonlinear absorption coefficients of **IEICO-4F** and **ITIC-4F** extracted from Z-scan measurement.

	IEICO-4F		**ITIC-4F**	
Wavelength (nm)	**I_0 (GW/cm2)**	**β_{eff} (10^{-12} m/W)**	**I_0 (GW/cm2)**	**β_{eff} (10^{-12} m/W)**
850	-	-	18.8	1.37
	-	-	37.6	1.81
	-	-	56.5	2.28
900	-	-	8.39	1.41
	-	-	16.0	1.85
	-	-	24.0	2.46
950	2.07	8.85	9.94	1.25
	9.94	9.97	19.9	1.76
	19.9	11.37	29.8	2.31
1030	5.59	2.89	5.59	0.97
	10.9	3.87	10.9	1.27
	16.4	5.02	16.4	1.62
1200	19.9	2.46	37.1	1.95
	37.1	3.57	47.1	2.32
	53.1	4.27	53.1	2.61
1300	7.37	2.72	14.4	0.09

	14.4	3.55	20.0	0.11
	20.0	4.35	36.8	0.19
1350	11.9	1.95	-	-
	21.5	2.41	-	-
	40.1	3.35	-	-
1400	9.67	1.21	-	-
	18.65	1.53	-	-
	29.01	1.92	-	-

References

1. G. Boudebs, S. Cherukulappurath, *Physical Review A* **2004**, *69*, 053813.
2. J. Y. Yang, Y. L. Song, Y. X. Wang, C. W. Li, X. Jin, M. Shui, *Opt. Express* **2009**, *17*, 7110.